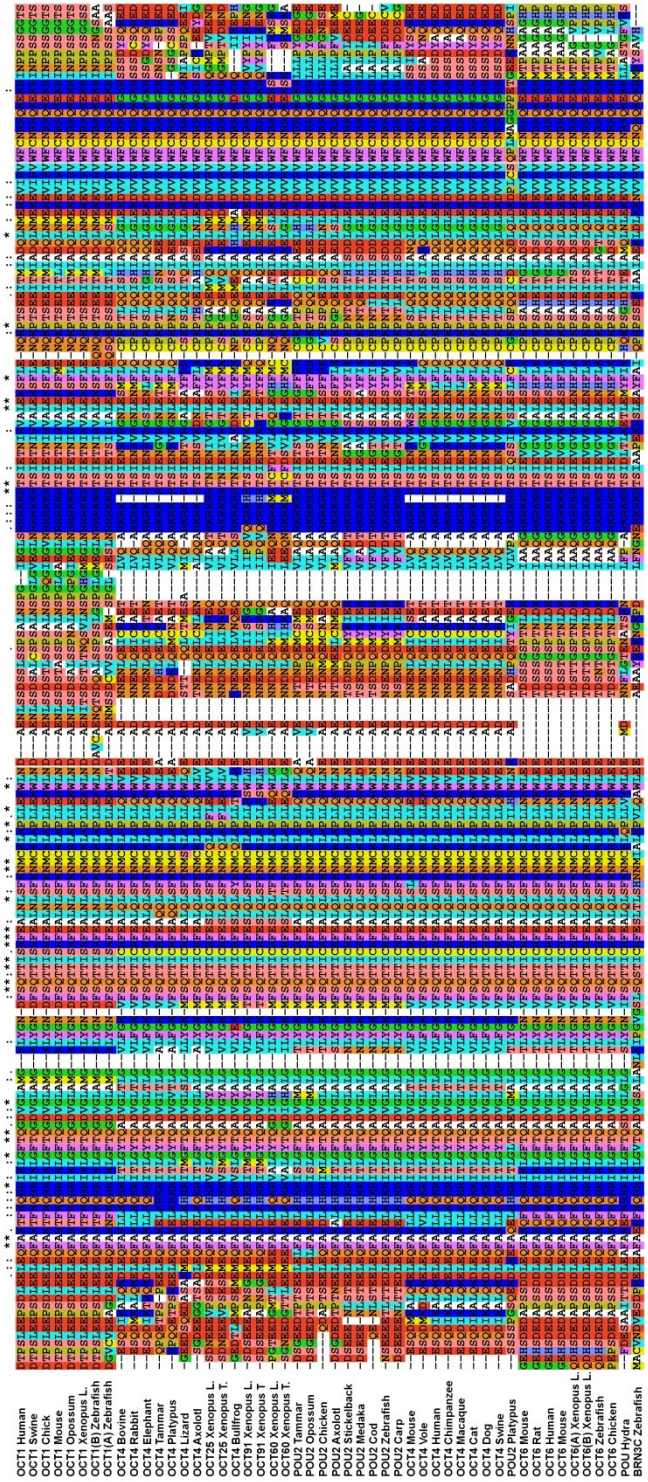

Supplementary Figure S1. Multiple Sequence Alignment of Pou2 and Oct4 Homologs.

Multiple sequence alignment of the DNA-binding domains of the POU factors used for the phylogenetic analysis. This alignment was used to generate the phylogenetic tree in Fig. 1A. The amino-acid color scheme is: LYS, ARG: dark blue; GLU, ASP: red; ALA: white; GLY: green; CYS, MET: yellow; SER, THR: pink; PHE, TYR, TRP: magenta; HIS: light blue; PRO: tan; ILE, VAL, LEU: cyan; ASN, GLN: orange.

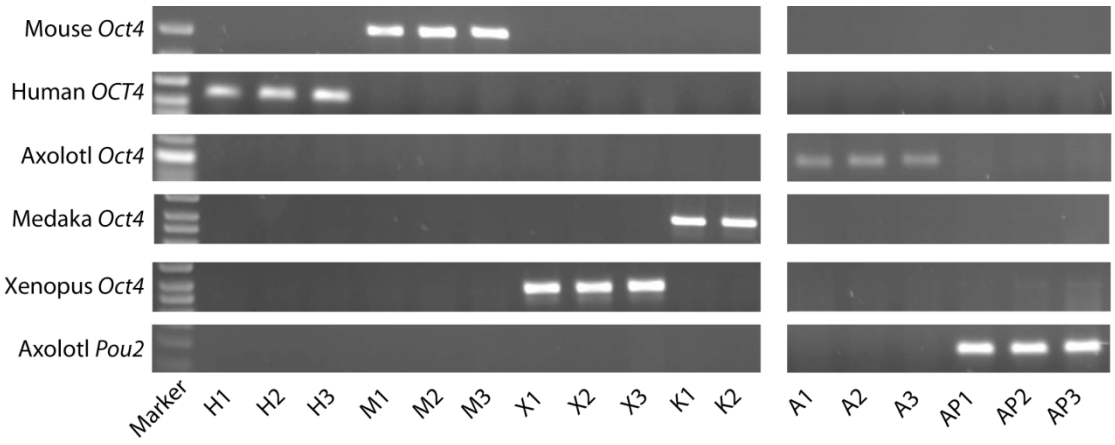

Supplementary Figure S2. Genotyping of the Mouse iPSC Colonies Reprogrammed Using the Different *POU* Homologs. Primers used for genotyping that can amplify only one specific POU homolog are indicated on the left. On the bottom, individual clones generated using the different *POU* factors are represented as: H (human *OCT4*), M (mouse *Oct4*), X (xenopus *Oct91*), K (medaka *Pou2*), A (axololt *Oct4*), and AP (axolotl *Pou2*). For each pair of primers, the clones containing the only POU homolog that can be specifically amplified are considered to be positive controls; the rest of the clones are considered to be negative controls. Amplicons for each specific pair of primers were loaded into two different gels as indicated.

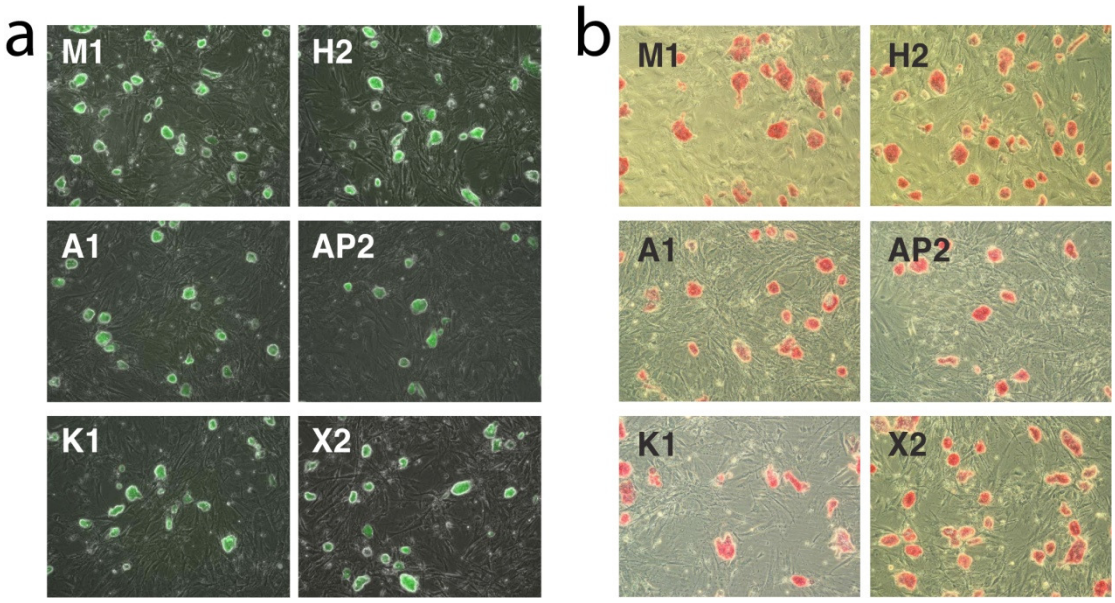

Supplementary Figure S3. Characterization of Generated Mouse iPSCs Using Different *POU* factors. For each *POU* factor, one iPSC clonal cell line is shown for GFP (**a**) and ALP expression (**b**).

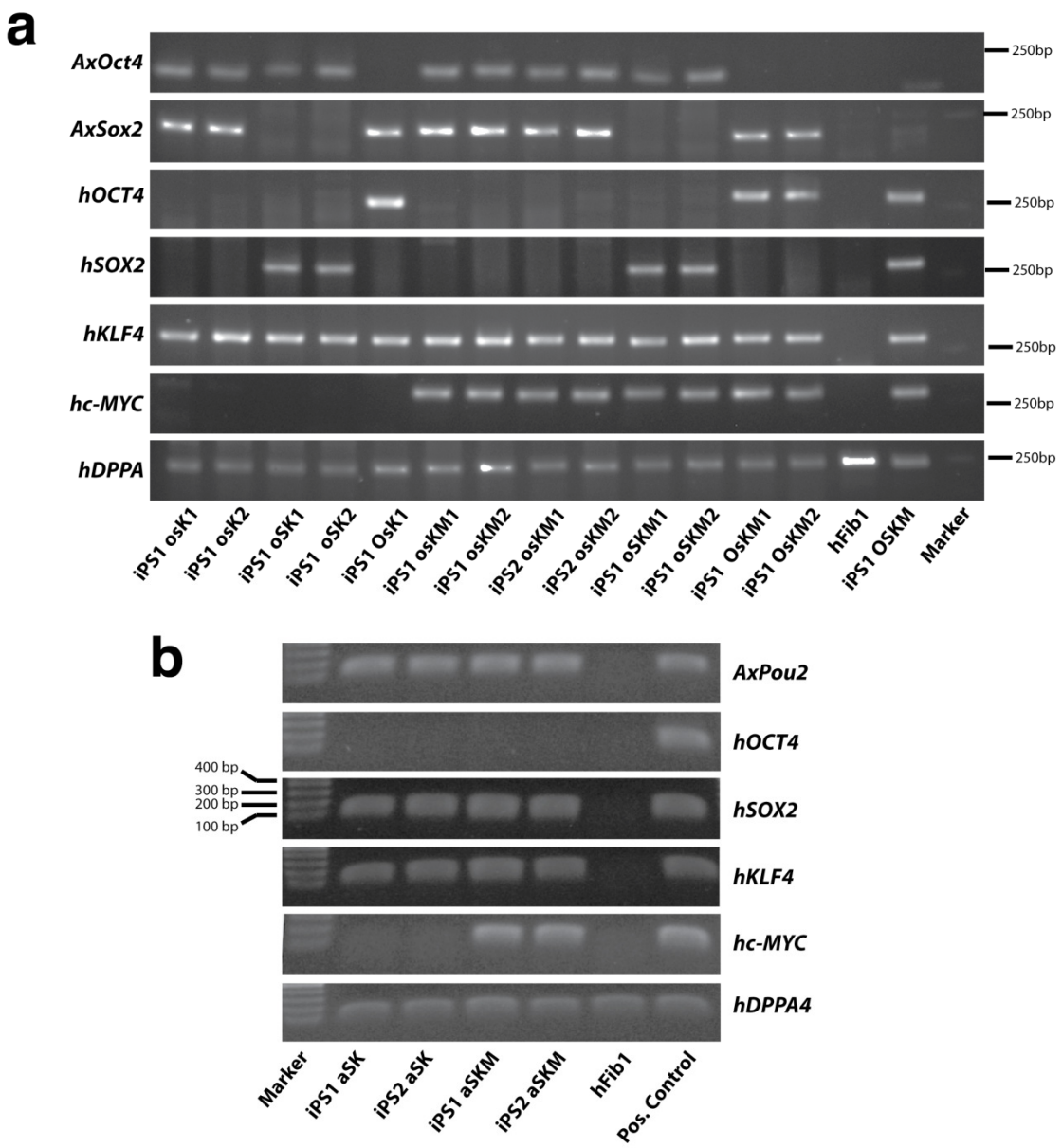

Supplementary Figure S4. Genotyping of Human iPSC Colonies Generated Using the Axolotl *Pou2*, Axolotl *Oct4*, and Axolotl *Sox2* Transcription Factors. Genomic PCR using specific primers for each viral vector was performed on human iPSCs generated using AxOct4 (**a**) or AxPou2 (**b**). *DPPA4* was used as a loading control. hFib1 was considered to be the negative control, while iPSCs generated with human factors (**a**) or the plasmids used for the viral preparation (**b**) were used as positive controls.

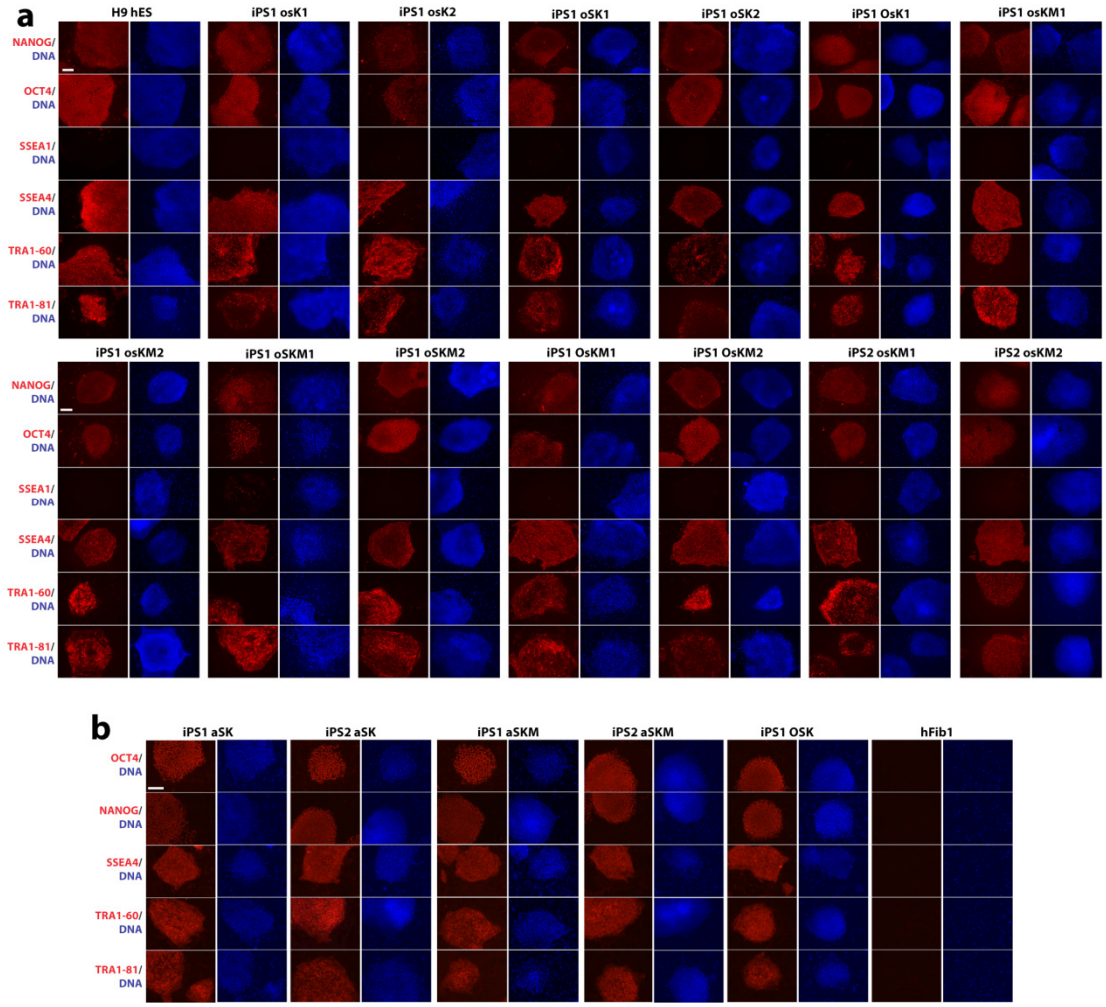

Supplementary Figure S5. Characterization of the Human iPSCs Generated Using the Axolotl *Pou2*, Axolotl *Oct4*, and Axolotl *Sox2* Transcription factors. Human pluripotency markers (*NANOG*, *OCT4*, *SSEA4*, *TRA1-60*, and *TRA1-81*) and a non-pluripotency marker (*SSEA-1*) were evaluated by immunohistochemistry in human iPSCs generated using AxOct4 (**a**) or AxPou2 (**b**). H9 human ESCs cells and iPS OSK cells were used as a positive control, while hFib1 were considered as the negative control. Nuclei were stained with Hoechst (blue). All pictures correspond to a 10X magnification. Scale bars represent 100 µm.

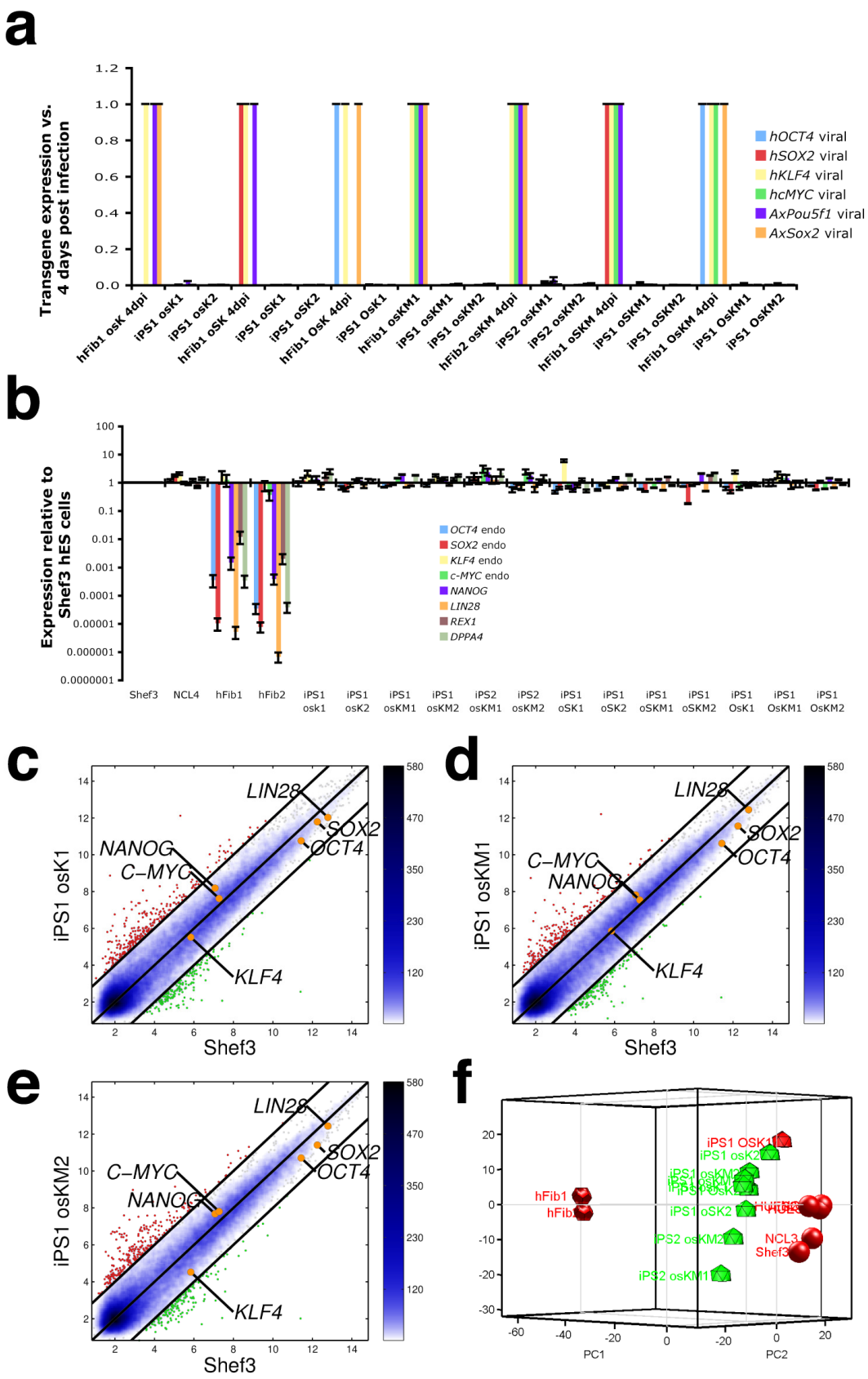

Supplementary Figure S6. Gene Expression Analysis of the Human iPSCs. (**a**) Expression level of the viral transgenes was measured in the human iPSCs by qRT-PCR using specific primers. Fibroblasts harvested 4 days after infection are used for comparison as a positive control. Error bars represent the standard error arising from using *GAPDH* and *ACTB* for normalization. (**b**) The expression levels of some pluripotency marker genes (*OCT4*, *SOX2*, *KLF4*, *C-MYC*, *NANOG*, *LIN28I*,

and *REX1*) were measured by qRT-PCR. Values are given as fold change compared with Shef3 hESC levels. NCL4 hESCs show the variation between different hESC lines. Error bars show the standard error arising from using *GAPDH* and *ACTB* as housekeeping genes. (**c**, **d**, **e**) Pairwise scatter plots with global gene expression profile comparing Shef3 hESCs with (**c**) iPS1 osK1, (**d**) iPS1 osKM1, and (**e**) iPS1 osKM2 cells. Black lines indicate two-fold changes in gene expression levels between the paired populations. The color bar on the right indicates the scattering density. Genes up- and down-regulated are shown in red and green circles, respectively. The position of the pluripotent markers, *OCT4*, *SOX2*, *NANOG*, *KLF4*, *LIN28*, and *C-MYC* is shown as orange circles. (**f**) Principal Component Analysis (PCA) of the microarray data. The symbols in the PCA are as follows: hFib populations as red dodecahedra, the hESCs (HUES2, HUES6, NCL3, and NCL4) as red spheres, the iPSCs generated using the axolotl factors (iPS1 osK2, iPS1 osK1, iPS1 osKM1, iPS1 osKM2, iPS2 osKM2, iPS2 osKM1, iPS1 oSK2, and iPS1 OsK2) as green icosahedra, and the iPSCs generated using only human factors (iPS1 OSK1) as red icosahedra.

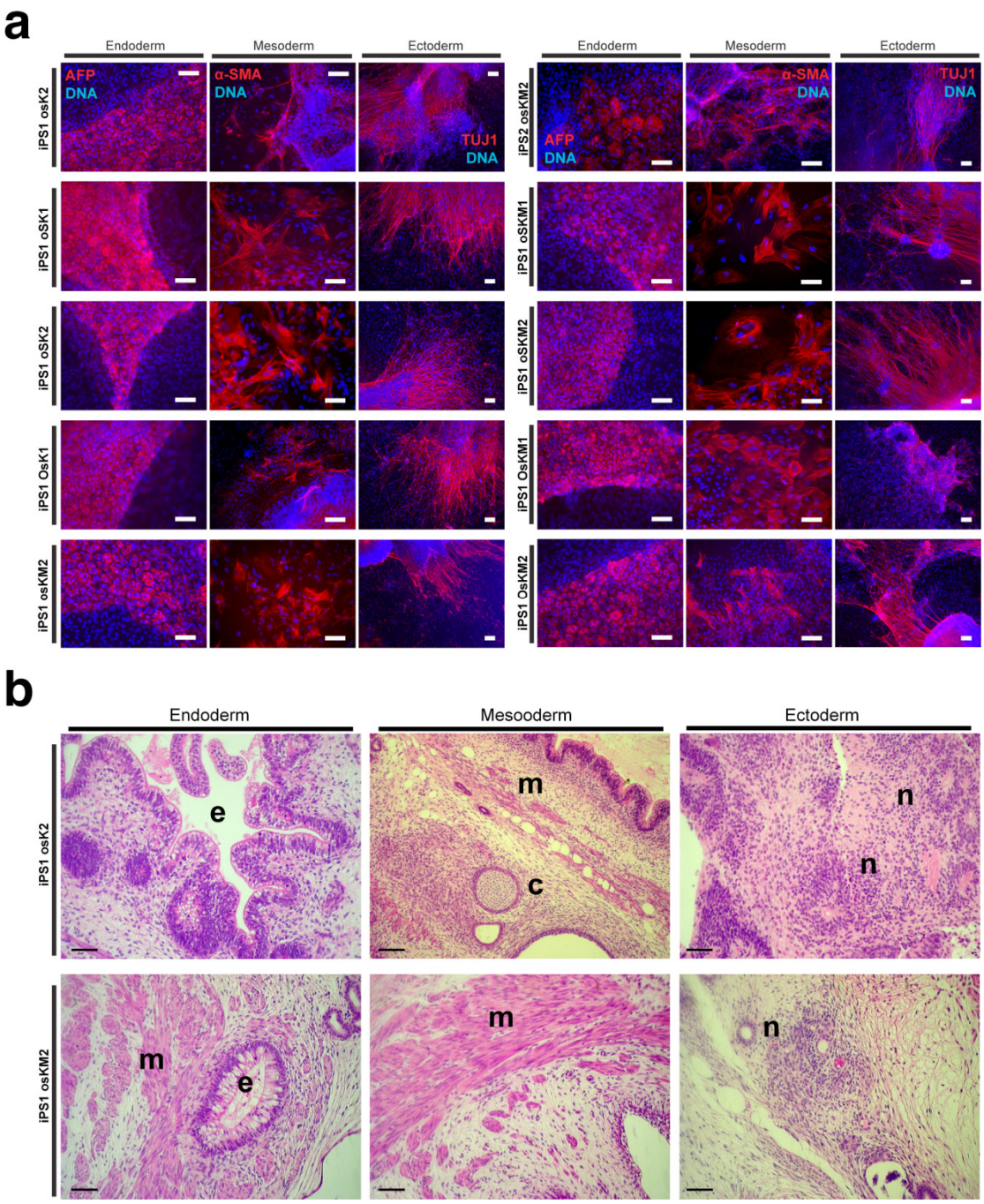

Supplementary Figure S7. *In Vivo* and *In Vitro* Pluripotency Analysis of the Human iPSCs. (**a**) *In vitro* differentiation of the axolotl iPSCs into cells of all three germ layers, shown by immunocytochemistry: endoderm (α-fetoprotein, AFP), mesoderm (α-smooth muscle actin, SMA), and ectoderm (β-Tubulin IIIb, TUJ1). Nuclei were stained with Hoechst (blue); scale bars, 250 µm. (**b**) Microsections of hematoxylin and eosin–stained teratoma generated 6–8 weeks after injecting nude mice with iPS1 osK 2 and iPS1 osKM 2 cells. The iPSCs developed into tissues of all three germ layers: endoderm (respiratory epithelium, **e**), mesoderm (skeletal muscle, **m**; cartilage, **c**), and ectoderm (neural epithelium with rosettes, **n**). Scale bars represent 100 µm.

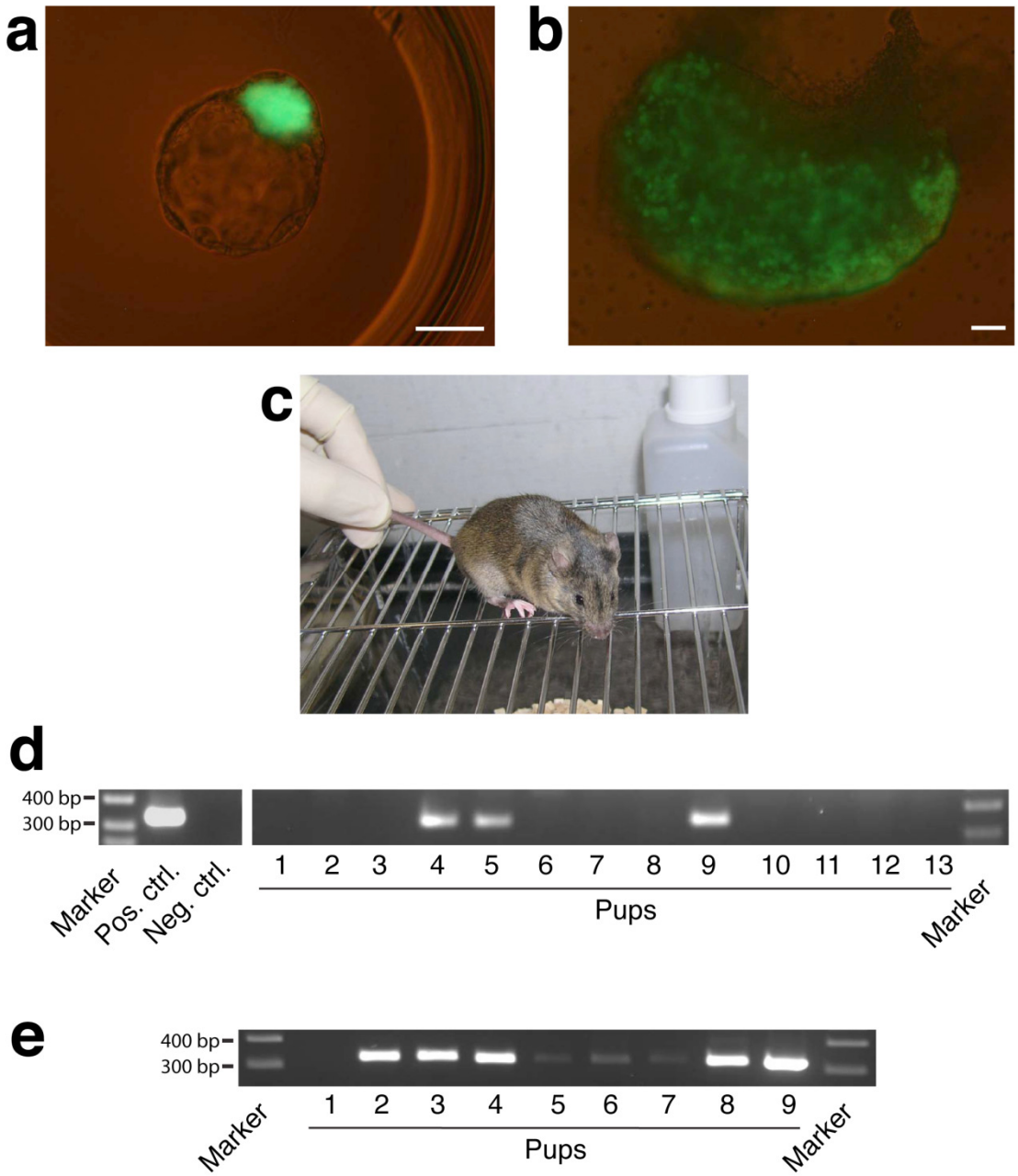

Supplementary Figure S8. Chimeric Contribution of the Mouse Axolotl *Oct4* iPSCs. (**a**) Blastocyst-stage embryo showing the integration of the *Oct4*-GFP–positive iPSCs into the inner cell mass. Scale bars represent 50 µm. (**b**) iPSC germline contribution into 12.5-dpc female gonads as shown by the presence of *Oct4*-GFP–positive germ cells. Scale bars represent 50 µm. (**c**) Mouse showing coat color chimerism. (**d** and **e**) Genotyping of the viral Klf4 in the F1 offspring generated from the first (**d**) and second (**e**) morula aggregation. The pMX-Klf4 plasmid was used as a positive control and non-infected MEFs were used as a negative control.

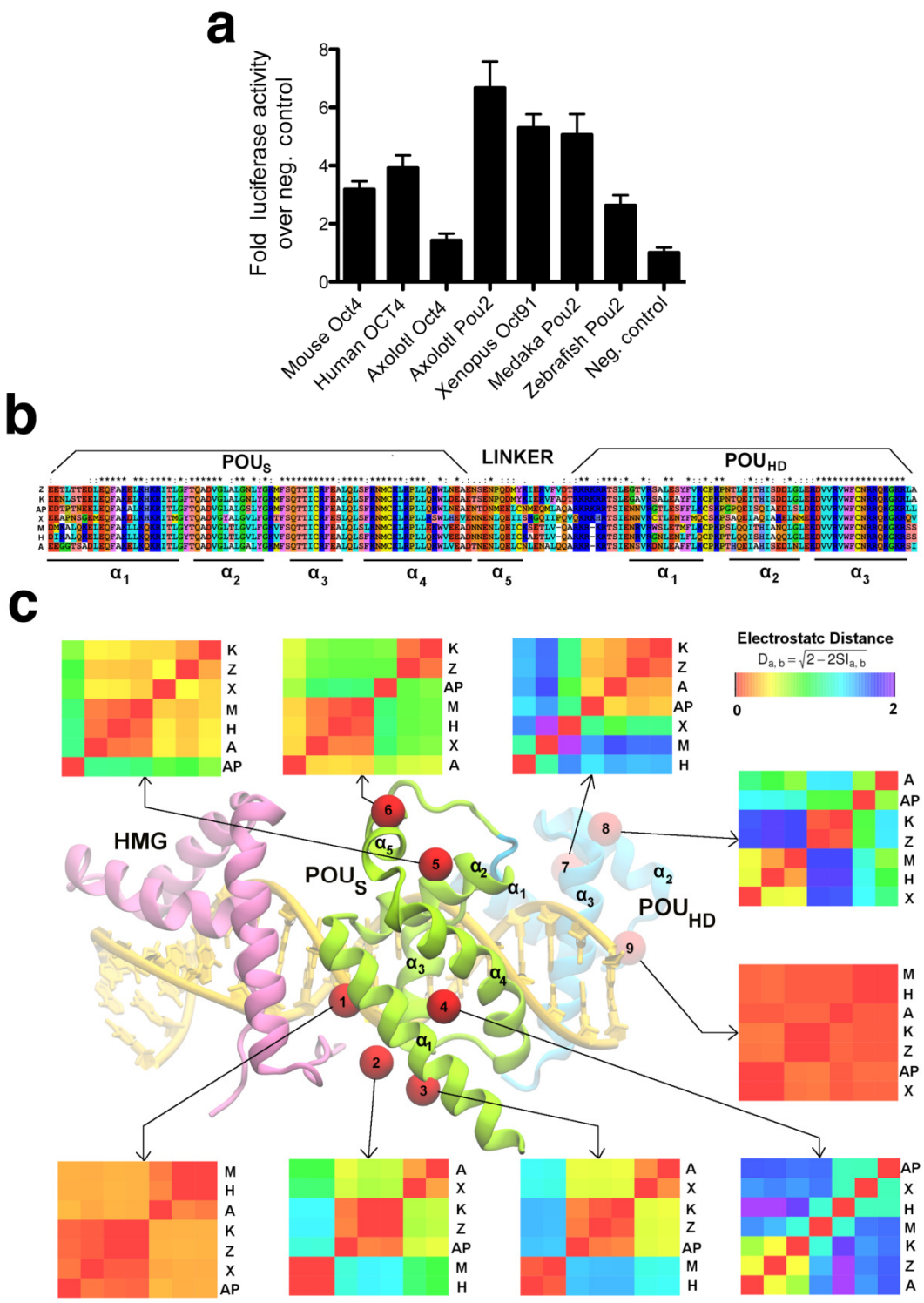

Supplementary Figure S9. Transcriptional Activity and Electrostatic Potential of the *POU* Orthologs. (**a**) The transactivation activity of the ortholog proteins was compared using the 37tk luciferase vector system and plotted relative to the levels of the negative control. Error bars reflect standard errors based on technical replicates. (**b** and **c**) Comparison of the structural models of *POU* orthologs. (**b**) Sequence alignment of the DNA-binding domains (POU_S and POU_{HD} connected by a linker region) of *POU* orthologs. The amino-acid color scheme is: LYS, ARG: dark blue; GLU, ASP: red; ALA: white; GLY: green; CYS, MET: yellow; SER, THR: pink; PHE, TYR, TRP: magenta; HIS:

light blue; PRO: tan; ILE, VAL, LEU: cyan; ASN, GLN: orange. (**c**) Comparison of the electrostatic potential of *POU* orthologs. The analysis was focused on different loci on the protein surface (numbered red spheres) corresponding to known or potential protein-protein interaction interfaces. For each locus, a map of the electrostatic distances between each pair of models was generated by hierarchical clustering (see Materials and Methods) and plotted as a heatmap colored from red (high similarity) to violet (high dissimilarity). The arrows indicate which map corresponds to which locus. For clarity, only the model of the human OCT4 is shown in ribbon representation. The POU_S and the linker are shown in light green, the POU_{HD} domain in light blue, and the HMG domain of SOX2 (known interacting partner of OCT4) in pink ribbons. The DNA is shown in yellow. A, Axolotl OCT4; AP, Axolotl POU2; X, Xenopus OCT91; K, Medaka POU2; Z, Zebrafish POU2; H, Human OCT4; M, Mouse OCT4.

Supplementary Table S1. Summary of Reprogramming Efficiency.

Factor combination	Wells seeded 2d after infection	No. of ES-like, AP-positive colonies / well	Reprogram-ming efficiency	weeks until first colonies
hFib1 OSK	50k	48 ± 11.1	0.34 ± 0.08	2-3
hFib1 OSKM	25k	190.3 ± 51.8	4.11 ± 1.12	1-2
hFib1 osK	50k 25k	3 2.5 ± 0.7	0.021 0.035 ± 0.01	5
hFib1 oSK	50k	9	0.064	4
hFib1 OsK	50k	29	0.21	3
hFib1 osKM	50k 25k	7 ± 1.4 7.5 ± 3.5	0.035 ± 0.01 0.16 ± 0.08	3-4
hFib1 oSKM	50k 25k	21 18	0.23 0.39	2-3
hFib1 OsKM	50k 25k	120 63	0.65 0.68	2
hFib2 OSKM	25k	98 ± 30.8	3.61 ± 1.14	1-2
hFib2 osKM	50k 25k	7.5 ± 3.5 6.5 ± 2.1	0.1 ± 0.013 0.24 ± 0.078	3-4
hFib1 aSK	25k 50k	5 ± 1.1 10.5 ± 2.1	0.11 ± 0.031 0.11 ± 0.023	3-4
hFib1 aSKM	12.5k 25k	8 ± 1.4 17 ± 2.8	0.63 ± 0.11 0.66 ± 0.11	2
hFib2 aSK	25k 50k	6 ± 4.2 13 ± 4.4	0.13 ± 0.09 0.28 ± 0.1	3-4
hFib2 aSKM	12.5k 25k	6 ± 1.4 12.5 ± 0.7	0.45 ± 0.11 0.47 ± 0.02	2

k, represents 10^3 cells.

The efficiency was calculated in all cases as 100 x number iPSC colonies / (percentage of cells expressing all the infected factors x total number of colonies). ALP+ corresponds to the number of ALP-positive colonies.

Supplementary Table S2. List of Primers Used for Cloning and Genotyping

Primer name	**Sequence (5'- 3')**
Axolotl-Pou2fl-BamHI-Fw	ACTGGATCCATGCTCGGAAGA
Axolotl-Pou2-NotI-Rv	AGAGCGGCCGCTTAGCTAATGCTG
Zebrafish-EcoRI-Fw	ATCGAATTCATGACGGAGAGAGC
Zebrafish-T-A-Rv	CCAAGCTGGTCCTTCGTTTTC
Zebrafish-T-A-Fw	GAAAACGAAGGACCAGCTTGG
Zebrafish-XhoI-Rv	TCGCTCGAGTTAGCTGGTGAGATG
Xenopus-BamHI-Pou91	ATCGGATCCATGTATAACCAACAG
Xenopus-XhoI-Pou91-Rv	TCGCTCGAGCTAGTTGCCTTGG
Medaka-Oct4-HindIII-Fw	GCACAAGCTTATGTCTGACAGG
Medaka-Oct4-NCBI-Rv	CTGTTGAAAGGTTCTCCTCCTCAGAGTCGC
Medaka-Oct4-NCBI-Fw	GCGACTCTGAGGAGGAGAACCTTTCAACAG
Medaka-Oct4-XhoI-Rv	TCGCTCGAGTCATCCTGTCAGGT
Oct4-RT-Fw3	GAGGCTGCAGCTGGAATTAG
Oct4-RT-Rv2	TATTCCAGGTATGGTGCAATAAAGT
*Sox2*_D_Fw1	ATGAAYGCITTYATGGTITGG
*Sox2*_D_Rv1	CRRTGCATIGGYTGCATYTG
*Sox2*_sRv1	AGCTGTCCATCCGCTGGCTGGAGTTCAT
*Sox2*_sFw2	GGCTACGGCATGATGCAGGAGCAGCT
*Sox2*_full_Fw	TTTCAAAAAAGTCTCCCGGAGTTGTCAAAA
*Sox2*_full_Rv	CGCTTAATCTCCTCTGTACAAAAATAGTCC
AxPou2R	CACGGTATCTCTTCCGAGCA
PouXenopusR	GGGTTGTGGGTAAAGGAAGG
PouMedakaR	GGAGTTGCCCAAACTTTCCT
AxOct4F	GAGATGTACTCGCAGACCGTGA
AxOct4R	CAATACTCAGTTGGAGTGCAGGTG
AxSox2F	CTGCGAGCAGTGAGCAGTCT
AxSox2R	GTTGTGCCTCTGGATTCAGTTGT
PouHumanF	GGCTCTCCCATGCATTCAAAC
PouHumanR	CATGGCCTGCCCGGTTATTA
pMXF	GACGGCATCGCAGCTTGGATACAC

Supplementary Table S3. Sequences Used for Alignment and Tree Building.

Genes/Species	Uniprot identifier / NCBI (GenBank) Accession code
Brn3c Zebrafish	Q90435 / NP_571353.1
Oct1 Human	P14859-1 / NP_002688.3
Oct1 Swine	F1S265 / NP_999429.1
Oct1 Mouse	P25425-1 / NP_035267.2
Oct1 Chick	P15143 / NP_990803.1
Oct1 Opossum	F7GF90 / -
Oct1 Xenopus Laevis	P16143-1 / NP_001095255.1
Oct1(A) Zebrafish	O42276 / NP_571513.1
Oct1(B) Zebrafish	A4IFW4 / NP_001082798.1
Oct6 Human	Q03052 / NP_002690.3
Oct6 Rat	P20267 / NP_620193.1
Oct6 Mouse	P21952 / NP_035271.1
Oct6 Chicken	O73861 / AAC18592.1
Oct6(A) Xenopus Laevis	P31363 / NP_001158054.1
Oct6(B) Xenopus Laevis	Q561L5 / NP_001096655.1
Oct6 Zebrafish	Q90482 / NP_571236.1
Oct4 Human	Q01860-1 / NP_002692.2
Oct4 Chimpanzee	Q7YR49 / NP_001238970.1
Oct4 Macaque	Q5TM49 / NP_001108427.1
Oct4 Cat	D3U664 / NP_001166912.1
Oct4 Dog	E2QTW5 / XP_538830.1
Oct4 Elephant	G3T5K8 / XP_003422494.1
Oct4 Rabbit	A2ICN2 / NP_001093427.1
Oct4 Swine	Q9TSV5 / NP_001106531.1
Oct4 Bovine	O97552 / NP_777005.1
Oct4 Rat	Q6MG27 / NP_001009178.1
Oct4 Vole	A0MPW0 / ABK34451.1
Oct4 Mouse	P20263 / NP_038661.2
Oct4 Tammar	D2EA24 / ACZ54717.1
Oct4 Platypus	A7X5W5 / NP_001229656.1
Oct4 Lizard	- / XP_003228387.1
Oct4 Axolotl	Q5J1Q2 / AAT09163.1
Oct4 Bullfrog	C1C4W5 / ACO52025.1
Oct25 Xenopus Laevis	Q7T103 / NP_001079832.1
Oct25 Xenopius Tropicalis	B3DM25 / NP_001123406.1
Oct60 Xenopus Laevis	Q91989 / NP_001081583.1
Oct60 Xenopus Tropicalis	B3DM23 / NP_001123836.1
Oct91 Xenopus Laevis	B7ZQA9 / NP_001081342.1
Oct91 Xenopus Tropicalis	F6TLT1 / XP_002942017.1
Pou2 Tammar	D2EA25 / ACZ54718.1
Pou2 Opossum	- / XP_003339690.1
Pou2 Stickleback	G3PZT5 / -
Pou2 Platypus	- / XP_001520175.1
Pou2 Chicken	A7Y7W2 / NP_001103648.1
Pou2 Medaka	Q6DVF4 / NP_001098339.1
Pou2 Carp	D3YBA7 / ADC96616.1
Pou2 Cod	Q2I0F8 / ABC84854.1
Pou2 Zebrafish	Q90270-1 / NP_571187.1
Pou Hydra	Reference Millane et al., 2011

SUPPLEMENTARY METHODS

Luciferase Assay

Dual-Glo Luciferase assay System (Promega) was used to measure the transactivation potential of the different *POU* orthologs. 4 x 10^5 293T cells were transfected with FuGENE 6 (Roche) in 24-well plates, following the manufacturer's instructions. Briefly, 100 ng of effector DNA (pMX coding for the different *POU* factors) was co-transfected with 10 ng of pTK-R, expressing Renilla luciferase, and 800 ng of the reporter construct, which drives the 37tk-Luciferase under the control of the canonical binding sequence for *POU* factors (the ATGCAAAT sequence repeated six consecutive times)[43]. Luciferase activity was measured in triplicates after 48 hours and normalized against the Renilla readout.

Comparison of the electrostatic potential of OCT4 orthologous

Comparative models of OCT4 orthologous were built using the following templates: (i) the structure of OCT4 bound as a homodimer on the *PORE* DNA (unpublished, PDBID: 3L1P); (ii) the structure of OCT1 bound as a heterodimer with the HMG domain of SOX2 on the *HOXB1* DNA[44] (PDBID: 1O4X); (iii) the structure of OCT1 bound as a heterodimer with the HMG domain of SOX2 on the *FGF4* DNA[45] (PDBID: 1GT0). First, 500 models of the human OCT4 were built to complete the structure of the linker between the DNA-binding domains, which was either unresolved or only partially resolved in the template structures. The structure of the linker was optimized using a loop refinement protocol that involved energy minimization as well as molecular dynamics simulations as implemented in MODELLER[46]. The best scoring model was selected and models for the other OCT4 orthologous were built using the selected model of human OCT4 as template. The final models were not refined to avoid any deviations from the template architecture that could introduce artifacts in the comparison of the electrostatic potentials. For each model, the electrostatic potential grid (dimensions in Å:129x129x129) was calculated with APBS[47] using the non-linear Poisson-Boltzmann equation at an ionic strength of 150 mM. The grids were compared with PIPSA using Hodgkin similarity indexes[48] and clustered using hierarchical clustering in R. In the PIPSA analysis, a skin of 5-Å thickness was built around the protein starting at its surface (estimated by the area accessible to a solvent probe of 1.5-Å radius). To focus the comparison at specific regions on the protein surface, 9 spheres of radius 8 Å were defined based on protein side chains (red spheres in Fig. 4). The electrostatic potential grids were compared in the regions where the skins of the models intersected each of the defined spheres.

SUPPLEMENTARY REFERENCES

43. Scholer, H.R., Ciesiolka, T. & Gruss, P. A nexus between Oct-4 and E1A: implications for gene regulation in embryonic stem cells. *Cell* **66**, 291-304 (1991).
44. Williams, D.C., Jr., Cai, M. & Clore, G.M. Molecular basis for synergistic transcriptional activation by Oct1 and Sox2 revealed from the solution structure of the 42-kDa Oct1.Sox2.Hoxb1-DNA ternary transcription factor complex. *J Biol Chem* **279**, 1449-1457 (2004).
45. Remenyi, A., *et al.* Crystal structure of a POU/HMG/DNA ternary complex suggests differential assembly of Oct4 and Sox2 on two enhancers. *Genes Dev* **17**, 2048-2059 (2003).
46. Sali, A. & Blundell, T.L. Comparative protein modelling by satisfaction of spatial restraints. *J Mol Biol* **234**, 779-815 (1993).
47. Baker, N.A., Sept, D., Joseph, S., Holst, M.J. & McCammon, J.A. Electrostatics of nanosystems: application to microtubules and the ribosome. *Proc Natl Acad Sci U S A* **98**, 10037-10041 (2001).
48. Wade, R.C., Gabdoulline, R.R., and De Rienzo, F. Protein Interacton Property Similarity Analysis. *Int J Quant Chem* **83**, 122-127 (2001).